Atomistic analysis of the annealing behavior of amorphous regions in silicon

Pedro López,[a] Lourdes Pelaz, Luis A. Marqués, and Iván Santos
Departamento de Electricidad y Electrónica, Universidad de Valladolid, E.T.S.I. Telecomunicación, Campus Miguel Delibes s/n 47.011 Valladolid, Spain

(Received 8 January 2007; accepted 9 March 2007; published online 10 May 2007)

We have analyzed the features of recrystallization of amorphous regions, using an atomistic amorphization-recrystallization model that considers the Si interstitial-vacancy pair as the building block for the amorphous phase. Both small amorphous pockets and large continuous amorphous layers are modeled as an accumulation of Si interstitial-vacancy pairs. In our model recrystallization is envisioned as a local rearrangement of atoms, the recrystallization rate of Si interstitial-vacancy pairs being determined by their local coordination. This feature explains the differences in the annealing behavior of amorphous regions with different topologies, the faster regrowth velocity of the damage tail compared with the continuous amorphous layer, and the independence of the regrowth velocity on the amorphous layer depth. © *2007 American Institute of Physics*. [DOI: 10.1063/1.2729468]

I. INTRODUCTION

The fabrication of ultrashallow junctions compatible with advanced complementary metal-oxide semiconductor (CMOS) technology requires a precise incorporation of a high dopant concentration near the surface. This is mainly achieved by high-dose low-energy ion implantation, which may produce self-amorphization of the implanted layer. In other cases, a preamorphizing implant is performed to take advantage of the amorphization benefits: reduction of ion channeling and high dopant activation with minimal dopant diffusion during low-temperature solid phase epitaxial regrowth (SPER) of the amorphized layer.[1] However, defects that remain after regrowth beyond the initial amorphous/crystalline (a/c) interface inject Si interstitials during subsequent thermal treatments causing dopant redistribution.[2]

The use of amorphization/recrystallization processes in the fabrication of integrated circuits drives the increasing demand for the development of predictive models. One of the most widespread amorphization models considers that the region being implanted turns amorphous when a critical defect concentration (CDC) is exceeded.[3] By comparing the experimental a/c interface position with theoretically generated damage profiles, CDC values can be estimated.[3] At cryogenic implant temperatures similar CDC values have been obtained for different ions,[4] but at room or higher implant temperatures, divergences of more than one order of magnitude were reported.[3] Different CDC values applied to the theoretical damage profile lead to variations in the predicted a/c interface depth, and this strongly affects the amount of residual damage beyond the interface.[5] The variety of CDC values reflects the different resistance of damage to annealing, and it has a noticeable effect when dynamic annealing is intense. Improved models require a better understanding of the mechanisms underlying the formation and recrystallization of amorphous regions, and to account for the dynamic annealing of damage during the implant.

It has been experimentally observed that continuous amorphous layers (a-layers) and amorphous pockets (a-pockets) exhibit similar annealing and structural features.[6–8] Transmission electron microscopy (TEM) images show that damage clusters present an amorphouslike appearance, and that regrowth starts at interfaces with the crystalline phase. Moreover, the influence of dopants and ion beam irradiation on the amorphization and recrystallization of planar a/c interfaces and a-pockets shows strong similarities.[7] However, experimental evidence indicates that a-pocket recrystallization is much faster than that of continuous a-layers.[8,9] The regrowth of continuous a-layers follows a well-defined activation energy while the regrowth of a-pockets is not uniquely defined. Even in the case of the well-characterized layer-by-layer regrowth of the planar a/c interface, there is no agreement about the atomic mechanisms responsible for this behavior. Some authors consider that recrystallization occurs by bond breaking and network rearrangement at the interface.[10] Williams and Elliman qualitatively explained the regrowth on the basis of nucleation and motion of kinks on [110] edges of the a/c interface.[11] Other authors suggest that the diffusion of intrinsic defects in amorphous or in crystalline regions leads to the reordering of atoms and finally to the a-layer regrowth.[12] If this were the case, the amorphous layer width and the presence of defect sinks would affect the regrowth kinetics. However, the experimentally measured regrowth velocity in a-layers as thick as 5 μm indicates that crystallization occurs at a constant rate, and it is the same as that obtained for shallower a-layers.[13] SPER velocity of a Si a-layer in bulk Si and in a thin Si layer on a SiO_2 substrate is also the same,[14] although the buried Si/SiO_2 interface has been proven to act as a sink for point defects. Molecular dynamics calculations also indicate that the regrowth of

[a]Corresponding author; Electronic mail: pedrol@ele.uva.es

a-pockets is independent of the presence of point defects and that SPER is mainly a local atomic rearrangement at the regrowing interface.[15]

In this work we use atomistic kinetic Monte Carlo simulations to gain insight into the relevant mechanisms associated with the annealing behavior of amorphous regions upon thermal treatment. Our simulations provide a unifying view of the regrowth of different amorphous structures and contribute to clarifying some intriguing features.

II. SIMULATION MODEL

Our atomistic simulations of ion implantation and annealing are based on the following scheme: implantation cascades are generated using the binary collision computer code MARLOWE,[16] and the defect evolution is followed with the nonlattice kinetic Monte Carlo diffusion code DADOS.[17] MARLOWE provides the coordinates of Si interstitials and vacancies produced in each cascade, resulting in different damage morphologies. Annealing at the implant temperature is carried out after each implantation cascade during a time defined by the implant flux. Then, a new cascade is added to the remaining damage until the specified fluence is reached.

Along with Si interstitials and vacancies and their clusters, we also consider the bond defect or interstitial-vacancy (IV) pair.[18,19] An IV pair can be formed during the collision processes in a ballistic cascade[20] and also when a Si interstitial and vacancy are within the interaction radius of each other,[19] instead of undergoing instantaneous annihilation. An IV pair consists of the local rearrangement of the bonds of two lattice atoms producing the five- and seven-membered rings characteristic of the amorphous phase. This defect has no excess or deficit of atoms, but it introduces disorder in the Si lattice.[18,19] We use the IV pair as the building block to describe the amorphous phase.[18] As DADOS is a nonlattice code, only point or extended defects are taken into account in the simulations and their positions do not necessarily correspond to actual lattice sites. Considering the amorphous Si density[21] and that each IV pair involves two disordered lattice atoms, the average distance between IV pairs is 3.42 Å. We have estimated that an IV pair can be surrounded by up to 26 neighboring IV pairs in a cubic volume defined by 3.86 Å (second neighbor distance) on each direction around the selected IV pair. An IV pair in a planar interface would have an average of 17 neighboring IV pairs, corresponding to those in the amorphous side plus those in the interfacial monolayer.[22]

IV pair recombination implies that atoms are relocated in their crystalline positions. In our model each IV pair is locally characterized by the number of neighboring IV pairs. The recombination rate of the IV pair decreases as the number of neighboring IV pairs increases, reflecting the difficulty of "amorphous atoms" to properly rearrange when they have fewer neighboring atoms in crystalline positions. We assign an activation energy for recombination of 0.43 eV to the isolated IV pair (0 neighbors), according to molecular dynamics calculations.[18] IV pairs in a planar a/c interface is given an activation energy corresponding to that of the experimental recrystallization velocity, 2.7 eV.[23] IV pairs embedded into an amorphous matrix (completely surrounded by neighboring IV pairs, and thus with full coordination) have an activation energy of 5 eV, coincident with the experimentally observed activation energy for crystal nucleation in amorphous Si.[24] Other coordination numbers have intermediate activation energies as shown in Fig. 1.

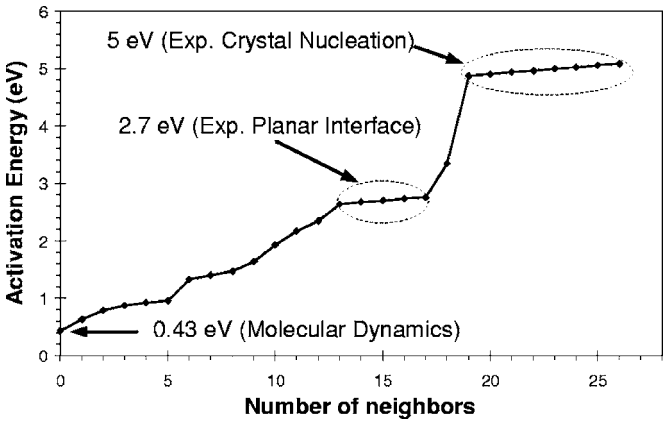

FIG. 1. Activation energies for the recombination of IV pairs as a function of the number of neighboring IV pairs.

In our model amorphous regions are considered as agglomerates of IV pairs. Thus, structural similarities of continuous a-layers and smaller a-pockets are naturally captured. The recrystallization probability of a given IV pair belonging to any amorphous region is determined by the distribution of surrounding IV pairs. IV pairs at an a/c interface have fewer neighboring IV pairs than those embedded within the amorphous region, and therefore recrystallization (IV pair recombination) will start at the interface. A continuous a-layer with a perfectly planar a/c interface is just a particular case of amorphous region, where all IV pairs at the interface have the same number of neighboring IV pairs and follow the same activation energy for regrowth, 2.7 eV. The recombination of the first IV pair at the planar interface starts a triggering mechanism in which its neighbors are the most likely ones to be recombined next since they have lost a neighbor (the one that has recombined first). This mechanism leads to the complete recrystallization of the whole monolayer. A new triggering event is required to start the regrowth of the next monolayer. Our model is similar to the nucleation and movement of kinks on [110] edges of the a/c interface proposed by Williams and Elliman.[11] The nucleation of a kink would correspond to the recombination of the first IV pair at the interface. The recrystallization of the neighboring IV pairs resembles the movement of the kink along the interface. The regrowth of a-pockets is more complex because they can exhibit a large variety of sizes and shapes; therefore, not all IV pairs at an interface have the same coordination number.

The experimental dependence of the SPER velocity on the local concentration of impurities within a-layers or a-pockets[25] could be also included in our model by considering that the IV pair recombination probability also depends on the concentration of neighboring impurities. Our present model does not consider the experimentally observed dependence of the regrowth kinetics on crystal orientation.[26]

We consider that any excess or deficit atoms contained in

the amorphous region are swept as IV pairs recombine and the interface advances. When an amorphous region completely recrystallizes, the unbalanced atoms are released to the crystal and they appear as Si interstitials or vacancies. Thus, residual Si interstitials are observed beyond the a/c interface after regrowth. Also, a band of defects appears where both interfaces of a buried a-layer meet.[27] When the a/c interface reaches the surface, the unbalanced defects are eliminated there.

III. RESULTS AND DISCUSSION

In this section we analyze different damage morphologies that may be obtained as a result of ion implantation. We present experimental results and provide a consistent explanation for them on the basis of our atomistic amorphization model. Atomistic models are a suitable tool for this goal because they can easily capture local differences in the damage morphology generated by implantation cascades.

A. Regrowth of individual a-pockets

It has been experimentally and theoretically demonstrated that individual cascades of heavy ions can cause the formation of rather extensive damage regions which have an amorphous appearance in TEM images. When analyzing those a-pockets individually, each of them showed different regrowing kinetics and even those with similar size regrew at different temperatures.[9,15,28] Analysis of a-pocket evolution with time show that the recovery of small amorphous zones is a two-step process, in which there is an initial fast shrinkage followed by a plateau and a latter fast regrowth that leads to the complete recrystallization of the a-pocket.[9] The combination of fast shrinkages and plateaus and the lack of an exponential decay indicates that the regrowth of a given a-pocket is not controlled by an unique activation energy.

In our model the irregular and convex shape of a-pockets translates into the existence of IV pairs at the interface with fewer neighboring IV pairs than those at a planar interface. This explains the faster recrystallization of a-pockets compared to that of a planar interface. The variations in the recrystallization kinetics of different amorphous pockets are captured by the local characterization of the recombination probability of IV pairs. To clarify this idea, we have simulated the recrystallization of three a-pockets with the same number of IV pairs but with different geometries. Though the interface of an a-pocket is generally irregular, to illustrate the regrowth behavior we have used two compact structures, a cube and a sphere, and also a star-shaped a-pocket, all of them with 512 IV pairs. Their longitudinal dimension is approximately 3 nm, similar to a-pockets observed as the result of Xe implants in Si.[9] Their evolution upon annealing with a time scale referred to the spherical a-pocket annealing time (the most stable one) is plotted in Fig. 2. In the insets we represent the schematics of IV pair structure for the three different geometries. It is clearly shown that, despite their identical size, the starlike a-pocket takes less than 15% and the cubelike a-pocket about 60% of the spherical a-pocket recrystallization time to completely regrow. IV pairs at the corners or "fingers" have fewer neighboring IV pairs and recombine quickly, shortening the lifetime of the a-pocket. An initial fast decay is observed in the cubical structure (from 512 to ~420 IV pairs) corresponding to atoms in the corners and edges of the cube, and also in the star-shaped structure corresponding to their fingers. Once the external IV pairs have recombined and a more compact structure is formed, the regrowth is slower. In the case of the sphere, all IV pairs at the interface see a similar and larger number of neighboring IV pairs than those in the other structures. Their activation energy is higher and therefore the recrystallization slower. Similar to experimental observations,[9] in all cases, there is a final fast decay since, in small a-pockets, IV pairs at the interface have few neighboring IV pairs even in compact geometries.

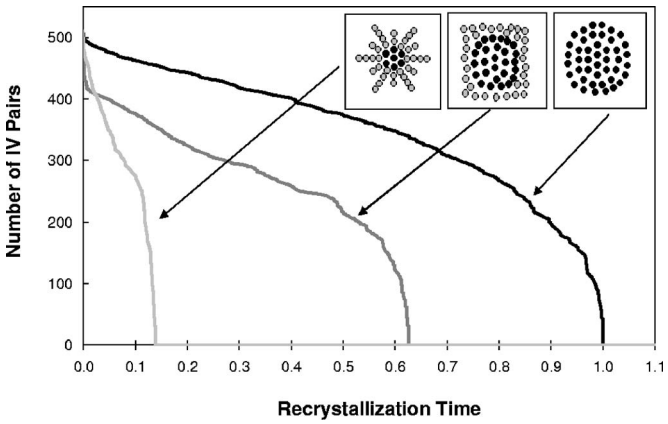

FIG. 2. Number of IV pairs of three different shaped a-pockets during annealing at 673 K. All a-pockets have initially the same size (512 IV pairs) but different geometries: a compact cube and a sphere, and a very irregular starlike a-pocket. In the insets we represent the IV pair structure for the three different geometries. Time scale is referred to the spherical a-pocket recrystallization time, considered as unity. The plot shows that the more irregular the geometry the faster the recrystallization. Fast decays and plateaus characteristic of the annealing of isolated amorphous regions can also be observed.

B. Regrowth of highly damaged regions

The initially fast damage recovery followed by a slower regrowth is also observed when analyzing as a whole the damage generated by ion implantation. Priolo *et al.* analyzed the evolution of the damage produced by 2×10^{13} cm^{-2} 150 keV Au ions implanted at liquid nitrogen temperature (LN_2T)), during annealing at 523 and 623 K for up to 2 h.[29] With these implant conditions no continuous a-layer was formed but the scattering yield of the Rutherford backscattering spectrum (RBS) reached 80% of the random level which revealed a high damage concentration. In the first 30 min of annealing at 523K RBS showed a significant damage reduction, but during the following 90 min there was hardly any damage recovery. When the annealing temperature was increased to 623 K a larger damage fraction recrystallized, but saturation was again observed. We have reproduced in our simulations the implant and annealing conditions used by Priolo *et al.* In Fig. 3 we plot their experimental results obtained by RBS and the simulated recrystallized fraction, considered as the ratio between the number of recombined IV pairs and the initial number of IV pairs. An initial fast re-

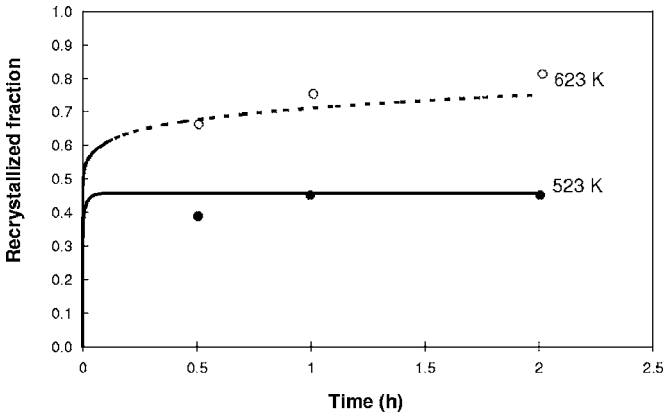

FIG. 3. Recrystallized fraction of a 2×10^{13} cm^{-2} 150 keV Au implant, when annealed at 523 and 623 K. Lines represent our simulation results, and symbols the experimental data from Ref. 29. Saturation is observed at both temperatures, the recrystallized fraction being higher at 623 K.

combination followed by a plateau or saturation in the amount of recombined IV pairs is clearly observed.

In Fig. 4 we plot the distribution of remaining IV pairs as a function of their coordination number after implant at LN_2T (77 K) and after annealing at different temperatures. During ion implantation the overlapping of damage regions from different cascades may lead to the formation of locally amorphous regions with a large variety of geometries and sizes. This implies the existence of IV pairs with different numbers of neighboring IV pairs and, therefore, different activation energies for recrystallization. At 77 K dynamic annealing during the implant is very low and most generated damage survives. IV pairs with a number of neighboring IV pairs ranging from 0 (isolated IV pair) to full coordination (IV pairs within larger amorphous regions) coexist in the sample. At room temperature (RT) dilute damage (IV pairs with few neighbors and therefore low activation energy for recombination) anneals out. At higher annealing temperatures more defects are eliminated and the remaining IV pair

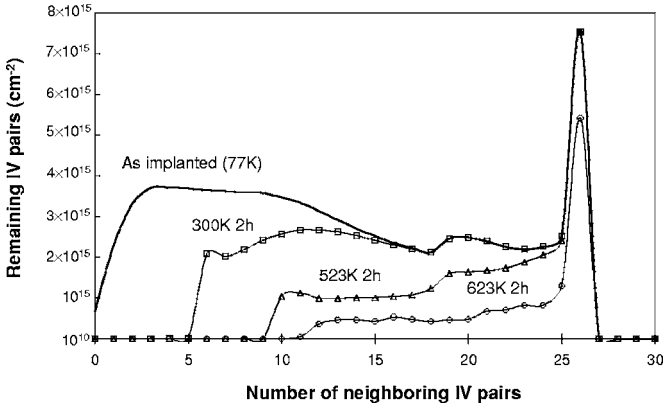

FIG. 4. Distribution of the remaining dose of IV pairs as a function of the number of neighboring IV pairs for the same conditions as in Fig. 3. The as-implanted case (at 77 K) and the distributions after annealing at several temperatures (300, 523, and 623 K for 2 h) are shown. At 77 K almost all generated damage survives: IV pairs with a number of neighboring IV pairs from 0 (isolated IV pair) to 26 (full coordination) are present in the sample. At RT dilute damage (IV pairs with few neighbors) anneals out. At higher annealing temperatures more stable damage is eliminated and the remaining IV pair distribution shifts toward the region of higher number of neighbors.

distribution shifts toward higher number of neighbors. In this thermally activated recombination process, IV pairs with energy barriers for recombination lower than ~1.7 eV easily recombine within 2 h at 523 K. An energy barrier increase of only 0.1 eV leads to a factor of ~9 longer for the recombination time at this temperature. Thus, after recombination of IV pairs with energy barriers lower than ~1.7 eV, recrystallization basically halts since the triggering event for recombination of the remaining structures would take too long at this temperature. At 623 K, energy barriers lower than ~2.3 eV can be overcome, and a larger fraction of defects is annealed out. Nevertheless, the amount of IV pairs with larger number of neighbors (larger energy barriers) also decreases compared to the distribution at RT because, as external IV pairs (those with lower number of neighbors) recombine, the neighboring number of IV pairs belonging to the next internal monolayer (which initially could have full coordination) is reduced and finally they may also recombine. At this temperature, an energy increase of 0.1 eV results in recombination times a factor of ~6.5 times longer. As reported in Fig. 3, the saturation is not so marked and a slow increase of the recrystallized fraction with time is observed at 623 K.

C. Regrowth of continuous a-layers and surrounding damaged regions

When damage created by ion implantation is accumulated until a continuous a-layer is formed, the surrounding regions are generally highly damaged too. By using TEM images and RBS, El-Ghor *et al.* analyzed the regrowth of a buried a-layer formed by a 1.25 MeV Si implantation at RT and LN_2T.[30] The LN_2T implant resulted in a wider a-layer than that generated in the RT implant. Quite sharp interfacial transition regions between the a-layer and the surrounding crystalline zones were observed for the RT implant, while a mixed-phase region (consisting of both amorphous and crystalline zones) surrounding the continuous a-layer was formed in the LN_2T implant. This mixed region was observed to anneal out at 673 K, a temperature too low for SPER of planar interfaces.

We have simulated the evolution upon annealing of the damage generated by 10^{15} cm^{-2} 5 keV Si implant at RT and LN_2T. We use a much lower energy in our simulations compared to that used in the described experiments because high implant energies and thick a-layers would involve a rather large simulation cell and a huge amount of defects in our atomistic amorphization model. Nevertheless, our simulation conditions can illustrate the differences in the formation and regrowth of a continuous a-layer and damage tail generated by RT and LN_2T implants. In Fig. 5 we show the atomistic damage profiles as implanted at RT or LN_2T, after annealing at 673 K for 2 h, and after annealing at 873 K for 5 s. In the RT implant an a-layer that extends from the surface up to ~18 nm is formed and the transition is rather sharp. Beyond the a/c interface the remaining damage is mostly in the form of small Si interstitial and vacancy clusters. For the same energy and dose, the LN_2T implant results in a slightly wider a-layer (~20 nm) and a rather large region beyond the a/c

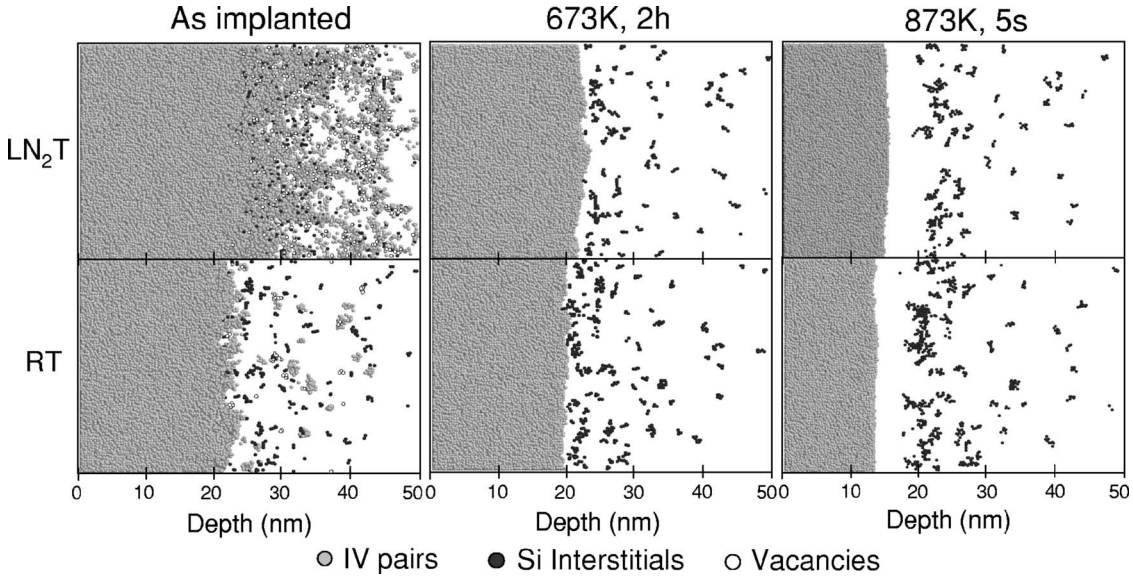

FIG. 5. Atomistic damage profiles for a 10^{15} cm^{-2} 5 keV Si implant at RT and LN_2T as implanted, after annealing at 673 K for 2 h and after annealing at 873 K for 5 s. After the implant at RT the a/c interface is abrupt, while at LN_2T there is a rather large region beyond the a/c interface that shows extensive amorphous regions mixed with nondamaged areas. Annealing at 673 K for 2 h removes the damage tail, but the regrowth halts as a very dense damage region near the a/c interface is reached. A higher annealing temperature is required to continue the regrowth of the continuous a-layer. During the regrowth residual damage is left beyond the initial a/c interface.

interface that shows extensive amorphous regions mixed with nondamaged areas. Annealing at 673 K for 2 h removes the damage tail, but the regrowth halts as a very dense damage region near the a/c interface is reached. A higher annealing temperature is required to continue the regrowth of the continuous a-layer.

Figure 6 shows the evolution upon annealing of the remaining IV pair dose distribution as a function of their coordination number for the RT and LN_2T implants. The profiles after annealing in both implants are very similar, with the main difference being the width of the a-layer (the height of the peak at 26 neighbors). The large fraction of IV pairs with 26 neighbors mostly corresponds to those inside the a-layer. Thus, the thicker a-layer generated for the LN_2T implant translates into a higher dose of IV pairs with 26 neighbors. The LN_2T implant also results in a wide neighboring distribution since all generated damage remains. However, for the RT implant isolated and small IV pair complexes are dynamically annealed during the implant itself (those with energy barriers lower than ~1 eV). Since Si ions do not produce very dense cascades, a significant fraction of the generated damage is annealed during the implantation. This makes the accumulation into extensive (and more stable) a-regions more difficult and, as a result, very little damage remains in the tail and the a-layer is thinner. When the implanted damage is annealed at 673 K the IV pair distribution is shifted toward a larger number of neighbors, as explained before, and most of the damage tail is annealed out. For a higher thermal budget (873 K annealing for 5 s) a planar a/c interface is formed and the remaining IV pairs show a bimodal distribution, belonging either to the bulk of the a-region (26 neighbors) or to the a/c interface (17 neighbors). There are also some IV pairs with coordination numbers similar to those of IV pairs in the regrowing layer or in the layer immediately below. As the a-layer regrows, the number of IV pairs at the interface remains approximately constant, whereas the number of IV pairs with 26 neighbors is reduced. The average configuration of IV pairs at the a/c interface is always the same and controls the regrowth. Thus, our model reproduces the layer-by-layer SPER and the independence of the regrowth velocity on the a-layer thickness and on the presence of point defect sinks in the crystalline region.

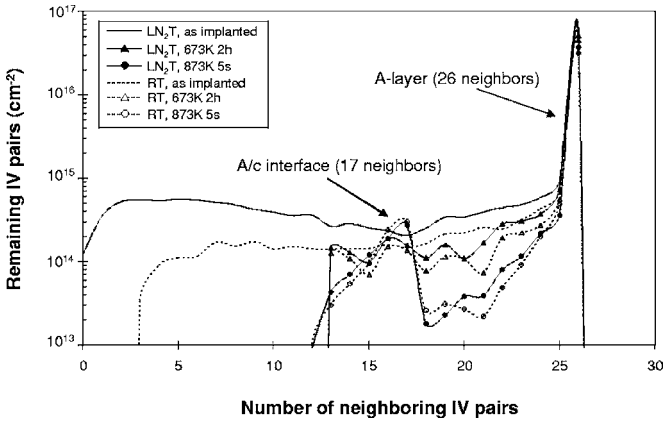

FIG. 6. Evolution upon annealing (673 K, 2 h and 873 K, 5s) of the distribution of the remaining dose of IV pairs as a function of the number of neighboring IV pairs for a 10^{15} cm^{-2} 5 keV Si implant at RT and LN_2T. Isolated and small IV pair complexes are dynamically annealed during the implant at RT, unlike the LN_2T case. The profiles after annealing in both implants are very similar, the main difference being the width of the a-layer (the height of the peak at 26 neighbors). During the regrowth of the continuous a-region (873 K, 5 s annealing) remaining IV pairs present a bimodal distribution, belonging mainly either to the bulk of the a-region (26 neighbors) or to the a/c interface (17 neighbors). As the annealing proceeds the number of IV pairs at the interface remains approximately constant, whereas the number of IV pairs contained in the a-layer is reduced.

IV. CONCLUSIONS

In this work we have analyzed the annealing behavior of amorphous regions in Si, ranging from a-pockets to continuous a-layers. We have used an atomistic amorphization and recrystallization model based on the IV pair as the building block for the amorphous phase. The recrystallization of amorphous regions is envisioned as the recombination of IV pairs whose rate is controlled by their local coordination. We have illustrated that the geometry is a key factor in the regrowth of a-pockets.

Differences in the stability of a-regions during annealing are explained on the basis of how IV pairs are distributed at interfaces: compact structures are more stable than irregular and convex interfaces in which IV pairs are surrounded to a large extent by crystalline Si (fewer neighboring IV pairs). When analyzing the regrowth of irregular a-pockets a fast shrinkage of the most protruding zones is observed, followed by a plateau once a compact structure is formed. Analogously, the annealing of ion implanted damage is characterized by a fast recovery of small and less stable a-pockets, followed by a slower regrowth of the denser damaged structures. The average local structure of IV pairs at a planar a/c interface is repeated layer by layer and controls the regrowth process independently of the thickness of the a-layer or the presence of defect sinks in the crystalline part of the interface.

ACKNOWLEDGMENTS

This work has been funded by the Spanish DGI under Project TEC2005–05101 and the JCyL Consejería de Educación y Cultura under Project VA070A05.

[1]M. Y. Tsai and B. G. Streetman, J. Appl. Phys. **50**, 183 (1979).
[2]M. Aboy, L. Pelaz, P. Lopez, L. A. Marqués, R. Duffy, and V. C. Venezia, Appl. Phys. Lett. **88**, 191917 (2006).
[3]G. Hobler and G. Otto, Mater. Sci. Semicond. Process. **6**, 1 (2003).
[4]K.-W. Wang, W. G. Spitzer, G. K. Hubler, and D. K. Sadana, J. Appl. Phys. **58**, 4553 (1985).
[5]I. Avci, M. E. Law, E. Kuryliw, and K. S. Jones, *IEDM Technical Digest* (IEEE, Piscataway, NJ, 2001), pp. 835–388.
[6]A. Battaglia, F. Priolo, E. Rimini, and G. Ferla, Appl. Phys. Lett. **56**, 2622 (1990).
[7]A. Battaglia, F. Priolo, C. Spinella, and E. Rimini, Nucl. Instrum. Methods Phys. Res. B **55**, 611 (1991).
[8]L. M. Howe and M. H. Rainville, Nucl. Instrum. Methods Phys. Res. **182–183**, 143 (1981).
[9]S. E. Donnelly, R. C. Birtcher, V. M. Vishnyakov, and G. Carter, Appl. Phys. Lett. **82**, 1860 (2003).
[10]F. Spaepen and D. Turnbull, in *Laser Annealing of Semiconductors*, edited by J. M. Poate and J. W. Mayer (Academic, New York, 1982).
[11]J. S. Williams and R. G. Elliman, Phys. Rev. Lett. **51**, 1069 (1983).
[12]J. Narayan, J. Appl. Phys. **53**, 8607 (1982).
[13]J. A. Roth, G. L. Olson, D. C. Jacobson, and J. M. Poate, Appl. Phys. Lett. **57**, 1340 (1990).
[14]J. J. Hamilton, E. J. H. Collart, B. Colombeau, C. Jeynes, M. Bersani, D. Giubertoni, J. A. Sharp, N. E. B. Cowern, and K. J. Kirkby, Nucl. Instrum. Methods Phys. Res. B **237**, 107 (2005).
[15]M.-J. Caturla, T. Diaz de la Rubia, and L. A. Marques, Phys. Rev. B **54**, 16683 (1996).
[16]M. T. Robinson and I. M. Torrens, Phys. Rev. B **9**, 5008 (1974).
[17]M. Jaraiz, L. Pelaz, J. E. Rubio, J. Barbolla, G. H. Gilmer, D. J. Eaglesham, H.-J. Gossman, and J. M. Poate, Mater. Res. Soc. Symp. Proc. **532**, 43 (1998).
[18]L. A. Marqués, L. Pelaz, J. Hernandez, J. Barbolla, and G. H. Gilmer, Phys. Rev. B **64**, 045214 (2001).
[19]M. Tang, L. Colombo, J. Zhu, and T. Diaz de la Rubia, Phys. Rev. B **55**, 14279 (1997).
[20]D. M. Stock, B. Weber, and K. Gärtner, Phys. Rev. B **61**, 8150 (2000).
[21]J. S. Custer *et al.*, Appl. Phys. Lett. **64**, 437 (1994).
[22]If IV pairs were distributed in a cubic lattice and separated by 3.42 Å, there would be 26 IV pairs around each IV pair in a cubic volume defined by the second neighbor distance on each direction around a central IV pair. Note that, although 27 IV pairs are considered in each capture volume, the Si density is kept because a given IV pair belongs to the capture volumes of different IV pairs. In terms of atomistic density, the contribution of each IV pair should be divided by the number of capture volumes it belongs to.
[23]G. L. Olson and J. A. Roth, Mater. Sci. Rep. **3**, 1 (1988).
[24]Y. Masaki, P. G. LeComber, and A. G. Fitzgerald, J. Appl. Phys. **74**, 129 (1993).
[25]G. L. Olson and J. A. Roth, *Handbook of Crystal Growth* (Elsevier, Amsterdam, 1994), Vol. 3, pp. 255–312.
[26]L. Csepregi, E. F. Kennedy, J. W. Mayer, and T. W. Sigmon, J. Appl. Phys. **49**, 3906 (1978).
[27]D. K. Sadana, M. Stratham, J. Washburn, and G. R. Booker, J. Appl. Phys. **51**, 5718 (1980).
[28]L. A. Marqués, L. Pelaz, P. Lopez, M. Aboy, I. Santos, and J. Barbolla, Mater. Sci. Eng., B **124–125**, 72 (2005).
[29]F. Priolo, A. Battaglia, R. Nicotra, and E. Rimini, Appl. Phys. Lett. **57**, 768 (1990).
[30]M. K. El-Ghor, O. W. Holland, C. W. White, and S. J. Pennycook, J. Mater. Res. **5**, 352 (1990).